Earth and Planetary Science Letters 384 (2013) 109–120

Contents lists available at ScienceDirect

Earth and Planetary Science Letters

www.elsevier.com/locate/epsl

Lava flow rheology: A comparison of morphological and petrological methods

M.O. Chevrel [a,*], T. Platz [b], E. Hauber [c], D. Baratoux [d], Y. Lavallée [a,e], D.B. Dingwell [a]

[a] Department of Earth and Environmental Sciences, University of Munich (LMU), Theresienstr. 41/III, D-80333 Munich, Germany
[b] Freie Universität Berlin, Institute of Geological Sciences, Planetary Sciences and Remote Sensing, Malteserstr. 74-100, 12249 Berlin, Germany
[c] German Aerospace Centre (DLR), Institute of Planetary Research, Rutherfordstr. 2, 12489 Berlin, Germany
[d] University Toulouse III, Institut de Recherche en Astrophysique et Planétologie (IRAP), UMR 5277 CNRS–UPS, 14, Avenue Edouard Belin, 31400 Toulouse, France
[e] Earth, Ocean and Ecological Sciences, University of Liverpool, Liverpool, L69 3GP, UK

ARTICLE INFO

Article history:
Received 10 October 2012
Received in revised form 23 August 2013
Accepted 13 September 2013
Available online 30 October 2013
Editor: T. Elliott

Keywords:
viscosity
yield strength
crystallisation sequence
morphology
Iceland
Mars

ABSTRACT

In planetary sciences, the emplacement of lava flows is commonly modelled using a single rheological parameter (apparent viscosity or apparent yield strength) calculated from morphological dimensions using Jeffreys' and Hulme's equations. The rheological parameter is then typically further interpreted in terms of the nature and chemical composition of the lava (e.g., mafic or felsic). Without the possibility of direct sampling of the erupted material, the validity of this approach has remained largely untested. In modern volcanology, the complex rheological behaviour of lavas is measured and modelled as a function of chemical composition of the liquid phase, fractions of crystals and bubbles, temperature and strain rate. Here, we test the planetary approach using a terrestrial basaltic lava flow from the Western Volcanic Zone in Iceland. The geometric parameters required to employ Jeffreys' and Hulme's equations are accurately estimated from high-resolution HRSC-AX Digital Elevation Models. Samples collected along the lava flow are used to constrain a detailed model of the transient rheology as a function of cooling, crystallisation, and compositional evolution of the residual melt during emplacement. We observe that the viscosity derived from the morphology corresponds to the value estimated when significant crystallisation inhibits viscous deformation, causing the flow to halt. As a consequence, the inferred viscosity is highly dependent on the details of the crystallisation sequence and crystal shapes, and as such, is neither uniquely nor simply related to the bulk chemical composition of the erupted material. This conclusion, drawn for a mafic lava flow where crystallisation is the primary process responsible for the increase of the viscosity during emplacement, should apply to most of martian, lunar, or mercurian volcanic landforms, which are dominated by basaltic compositions. However, it may not apply to felsic lavas where vitrification resulting from degassing and cooling may ultimately cause lava flows to halt.

1. Introduction

Morphological dimensions of lava flows are commonly used in planetary sciences to infer the rheological properties (viscosity, yield strength) of the erupted material, which are in turn used to estimate the silica content of the lava. Simple isothermal models of lava flow emplacement have been used to extract these properties, and the assumption has typically been made that lava flows have a single viscosity value. At first, Nichols (1939) proposed the Jeffreys' equation (Jeffreys, 1925) to calculate the viscosity of a lava flow from its dimensions assuming that it exhibits a Newtonian response. Recognising that lava may no longer behave as a Newtonian fluid as it cools, but may follow a Bingham law, a method was later proposed by Hulme (1974) to estimate the lava yield strength from its morphological dimensions. Experiments with analogue materials having a known rheological behaviour confirm that the morphology of a lava flow may be used to infer the rheology (e.g., Fink and Griffiths, 1992; Gregg and Fink, 1996, 2000; Lyman et al., 2004). Furthermore, according to the studies of Walker et al. (1973), Hulme (1974) and Pinkerton and Wilson (1994), and Moore et al. (1978), some linear relationship can be drawn between the viscosity or the yield strength and the bulk silica content. In recent decades, with the release of high-resolution images and topographic data of planetary surfaces, in particular for Mars, this approach has been largely used (e.g., Zimbelman, 1985, 1998; Wilson and Head, 1994; Baloga et al., 2003; Glaze et al., 2003; Glaze and Baloga, 2006; Hiesinger et al., 2007; Vaucher et al., 2009; Wilson et al., 2009; Hauber et al., 2011;

* Corresponding author.

0012-821X
http://dx.doi.org/10.1016/j.epsl.2013.09.022

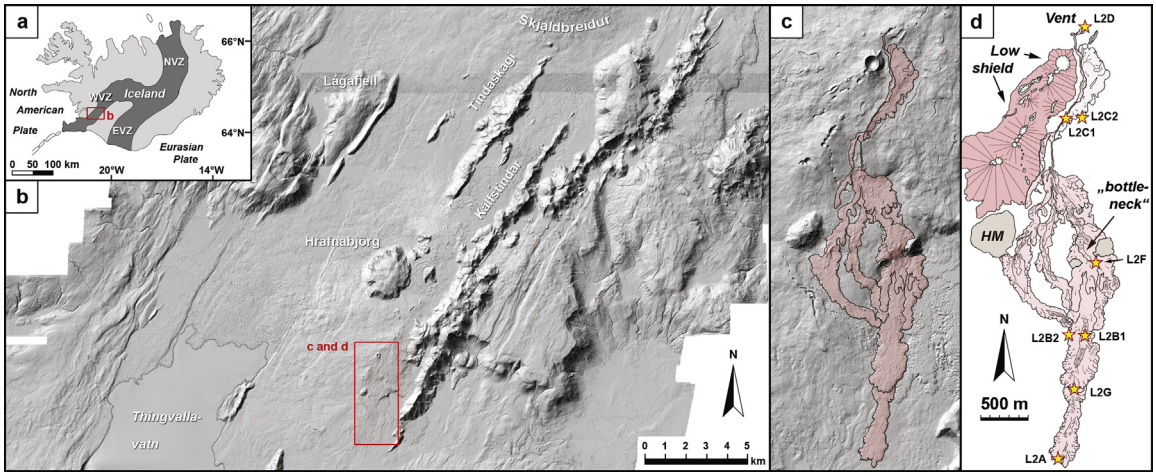

Fig. 1. (a) Location of the Western Volcanic Zone (WVZ) in Iceland; (b) Shaded elevation model of the area acquired with the HRSC-AX camera and location of the lava flow. (c) Highlight of the lava flow on the Data Elevation Model; (d) Map of the lava flow (light pink) and location of the sampling.
*HM (Hyaloclastite Mounds).

Jaeger et al., 2010; Pasckert et al., 2012; and references therein). Estimates of lava viscosities on Mars range from 10^2 to 10^8 Pa s and would appear to be consistent with basaltic to andesitic compositions.

The approximation of a single viscosity value neglects important physico-chemical processes, which are expected to affect considerably the rheology of lava (e.g., Shaw, 1969; Ryerson et al., 1988; Crisp et al., 1994; Cashman et al., 1999). For example, during emplacement of basaltic lava flow, heat loss induces crystallisation and consequently changes in the residual liquid composition, which both may increase the apparent viscosity of the flow by several orders of magnitude from the vent to the point where the flow halts. Moreover, under some compositional conditions, Giordano et al., 2007 showed that the concept of a rheological cut-off provides a rheological proxy for flow emplacement temperature. During lava flow emplacement, the viscosity of lava is therefore transient, and further evaluation of the validity of interpretations made from morphological methods is imperative.

The understanding of silicate melt rheology has rapidly advanced in the last three decades; a description of the rheology of silicate liquids as a function of temperature and chemical composition is now available (e.g., Hess and Dingwell, 1996; Dingwell, 2006; Giordano et al., 2008; Hui and Zhang, 2007). A reasonable understanding of the rheological contributions of crystals (e.g., Ryerson et al., 1988; Pinkerton and Stevenson, 1992; Lejeune and Richet, 1995; Pinkerton and Norton, 1995; Saar et al., 2001; Sato, 2005; Ishibashi and Sato, 2007; Caricchi et al., 2007; Costa, 2005; Costa et al., 2009; Petford, 2009; Ishibashi, 2009; Mueller et al., 2010; Castruccio et al., 2010; Vona et al., 2011; Cimarelli et al., 2011), bubbles (Bagdassarov and Dingwell, 1992; Lejeune et al., 1999; Stein and Spera, 2002; Manga et al., 1998; Saar and Manga, 1999), and their combined effects (Bagdassarov et al., 1994; Stein and Spera, 1992; Lavallée et al., 2007, 2012; Harris and Allen, 2008; Pistone et al., 2012) is emerging. Yet, it is well accepted that the rheological impact of particles is considerable and cannot be neglected. Their effect on viscosity is described by contributions to the Newtonian behaviour as well as the onset of non-Newtonian effects. The rheology of magmatic suspensions, with its phenomena of strain and strain-rate dependence, thus generally requires a non-Newtonian description. Complexity in describing the non-Newtonian nature has led to the proposal that above a critical crystal fraction, the rheology may be simplified to a Bingham fluid (e.g., Ryerson et al., 1988; Pinkerton and Stevenson, 1992) defined by its yield strength, which is dependent on crystal fraction. Despite recent experiments on multiphase magmas challenged the existence of yield strength (Lavallée et al., 2007; Caricchi et al., 2007), the concept persists in lava flow modelling because it enables computational simplifications.

How robust then, is the description of lava flow morphology in terms of a single rheological parameter (either viscosity or yield strength) reflecting the chemical composition and crystallisation sequence associated with a particular cooling history? To address this question, we focus here on a 4000-year-old basaltic lava flow from the Western Volcanic Zone in Iceland. Our approach combines (1) the determination of the rheological parameters from high-resolution morphological analysis, and (2) the determination of the rheological evolution of the lava according to its crystallisation sequence from eruption until complete crystallisation using petrographic analysis. The applications of our results to planetary data ought to be feasible as volcanic flows on Mars, the Moon and Mercury are dominated by basaltic compositions (BVSP, 1981).

2. Methods

2.1. Morphological analysis

2.1.1. Topographic imaging

In 2006, HRSC-AX, an airborne version of the High Resolution Stereo Camera (HRSC) on board Mars Express, was used for the acquisition of stereo and colour images of the Western Volcanic Zone, Iceland (Fig. 1). The HRSC-AX is a multi-sensor push-broom instrument with 9 CCD line sensors and has a stereo capability, which can systematically produce high-resolution Digital Elevation Models (DEMs). The principles of HRSC-AX data processing are similar to that of Mars Express-HRSC processing (see Scholten et al., 2005; Gwinner et al., 2010). The orientation data of the camera is reconstructed from a GPS/INS (Global Positioning System/Inertial Navigation System). The ortho-images have a map-projected resolution of 25 cm/pixel, and the DEM has a vertical resolution of 10 cm, an absolute accuracy of ~20 cm, and a horizontal grid spacing of 1 m.

2.1.2. Extracting rheological parameters from morphological dimensions

The following equations apply to the emplacement of cooling-limited lava flows in a laminar fashion with no inflation. All parameters used for the following equations are given in Table 1. The lava flow length (L) is related to its velocity (u) via the dimensionless Grätz number, (G_Z; Knudsen and Katz, 1958; Guest et al.,

Table 1
Notation of all variables.

Variable	Unit	Definition
G_z		Grätz number
u	$m\,s^{-1}$	Mean flow velocity
L	m	Length of the lava flow
κ	$m^2\,s^{-1}$	Thermal diffusivity
d_e	m	Equivalent diameter of the flow
Q	$m^3\,s^{-1}$	Volumetric effusion rate
H	m	Flow height
W	m	Flow width
w	m	Flow width minus widths of the channel's stationary levees
ρ	$kg\,m^{-3}$	Lava density
g	$m\,s^{-2}$	Gravitational acceleration
α	°	Slope of the underlying surface
n		Constant set to 4 for narrow flows
$\eta_{flow,1}$	Pa s	Flow viscosity from Jeffreys' equation
$\eta_{flow,2}$	Pa s	Flow viscosity from Warner and Gregg (2003)
$\eta_{flow,3}$	Pa s	Flow viscosity considering channelised lava flow
$\tau_{0,flow,1}$	Pa	Yield strength considering the underlying slope
$\tau_{0,flow,2}$	Pa	Yield strength considering the lateral spreading
$\tau_{0,flow,3}$	Pa	Yield strength considering channelised lava flow
η_{app}	Pa s	Apparant viscosity of polydispersed particle mixture
η_{melt}	Pa s	Viscosity of the interstitial silicate melt
η_r		Relative viscosity (effect of particles)
$\tau_0(\phi)$		Yield strength calculated as a function of crystal fraction
T	°C or K	Temperature
χ	wt.%	Chemical composition
ϕ		Particles' volume fraction
r		Particles' aspect ratio
$\dot{\gamma}$	s^{-1}	Strain-rate
ϕ_m		Maximum random packing fraction
B		Einstein coefficient (or intrinsic viscosity); $B\phi_m = 2.5$
ϕ_c		Volume fraction of coarse particle
ϕ_f		Volume fraction of fine particle
ϕ_*		Critical solid fraction at the onset of the exponential increase
ξ, γ, δ		Empirical parameters that vary with strain-rate and particles shape
x		Relative amount of finer particles with regard to coarser particles

1987; Pinkerton and Wilson, 1994), which considers the ratio of heat advection along the flow length to conductive heat losses:

$$G_z = \frac{u d_e^2}{\kappa L} \tag{1}$$

Several studies have described the relationship between effusion rates and flow lengths (Walker, 1973; Pinkerton, 1987; Pinkerton and Wilson, 1994; Pinkerton and Sparks, 1976) and concluded that cooling-limited flows halt when G_z falls to a critical value of 300. The volumetric effusion rate, Q, of the extruded lava is related to the velocity by:

$$Q = uWH = \frac{G_z \kappa L W}{H} \tag{2}$$

Assuming a Newtonian behaviour, the lava flow's geometry on an inclined surface depends on its viscosity, density, effusion rate, and the force that drives the flow (i.e., gravity), and is given by the Jeffreys' equation and later modified by Nichols (1939):

$$\eta_{flow,1} = \frac{\rho g H^3 W \sin\alpha}{nQ} \tag{3}$$

A simplified equation that omits the effect of lateral extent of the flow and of the slope was later proposed by Warner and Gregg (2003):

$$\eta_{flow,2} = \frac{\rho g H^4}{Q} \tag{4}$$

Results of Eqs. (3) and (4) generally agree if the flow does not develop levees and if the flow width is considerably larger than the flow height (Moore and Schaber, 1975).

Alternatively, assuming a Bingham behaviour, Hulme (1974) relates the yield strength of the flow to its geometric parameters according to:

$$\tau_{0,flow,1} = \rho g H \sin\alpha \tag{5}$$

The yield strength can also be calculated using the lateral spreading of the Bingham fluid, which is independent of the topographic gradient in the flow direction:

$$\tau_{0,flow,2} = \frac{\rho g H^2}{W} \tag{6}$$

In the context of channelised lava flows, Hulme's equations may be written as:

$$\tau_{0,flow,3} = \rho g (W - w) \sin^2\alpha \tag{7}$$

and

$$\eta_{flow,3} = \frac{w^3 \tau_{0,flow,3} \sin^2\alpha}{24Q} \quad \text{with } \frac{w}{W-w} < 1 \tag{8}$$

2.2. Sampling and analytical methods

One particular lava flow was selected within the area surveyed by the HRSC-AX camera in the Western Volcanic Zone, Iceland (Fig. 1). This lava flow is part of the Thjófahraun volcanic unit, resulting from the late phase of a fissure eruption event, dated at approximately 4000 yr B.P. (Sinton et al., 2005; Eason and Sinton, 2009). It was chosen because it has a main straight flow suited for evaluating the geometrical parameters. Moreover it is easily accessible for sampling and ground-truthing of remote sensing interpretations. Eight samples were selected at several distances from the vent to the flow front (Fig. 1d). For two sampling sites, pairs of samples were collected from the flow margin and centre (L2B1–L2B2 and L2C1–L2C2). Specimens from the flow top and outer margins were obtained, but the interior and the base of the flow could not be reached due to the lack of crevasses. Bulk rock geochemical analyses of five samples were carried out. Quantitative elemental analysis and back-scattered electron images were collected. Single images acquired with a polarised microscope were merged to portray the entire thin sections. Vesicles and crystals larger than 200 μm were colourised in an area of ~1000 × 1000 pixels. The resulting images were then processed by colour threshold separation for each phase using ImageJ (http://rsb.info.nih.gov/ij/). The proportion of vesicles and crystals are obtained by area pixel counting on binary images (crystal counts are done on a bubble-free area).

2.3. Crystallisation sequence

The crystallisation sequence was determined by petrographic observations. The modal abundance of each phase as a function of temperature was then determined using the thermodynamic calculator MELTS (Ghiorso and Sack, 1995). MELTS calculates via minimisation of the Gibbs free energy the composition and proportions of solids and liquids at thermodynamic equilibrium for prescribed pressure–temperature path and oxygen fugacity constraints. The crystallisation sequence was run in three steps to simulate the eruptive history of the lava from (i) phenocryst crystallisation in the magma chamber, to (ii) adiabatic ascent, and (iii) cooling and microcrystallisation at the surface. Crystallisation in the magma chamber was simulated by decreasing the temperature from the liquidus to the eruption temperature at a constant

pressure of 1 kbar and 0.4 wt.% H_2O as given by Eason and Sinton (2009). The eruption temperature is constrained by the temperature that is modelled by MELTS to achieve the crystallinity of the phenocryst assemblage as observed in the thin sections. Crystallisation induced during magma ascent (due to magma devolatilisation) was simulated using isothermal conditions and a pressure gradient from magma chamber conditions to the surface pressure of 1 bar. [Note: The decrease in temperature due to adiabatic decompression was neglected.] Finally, the cooling of the lava flow at the surface was simulated from eruptive temperature to complete crystallisation, using a pressure of 1 bar. The oxygen fugacity was held constant at two log units below the QFM buffer (QFM-2) in all steps (Eason and Sinton, 2009).

2.4. Viscosity modelling from petrographic analysis

The apparent viscosity of a polydispersed particle mixture (crystals and bubbles of various shapes and sizes) in a liquid phase (the silicate melt) may be defined by:

$$\eta_{app} = \eta_{melt}\eta_r = \eta_{melt}(T, \chi) \times \eta_r(\phi, r, \dot{\gamma}) \tag{9}$$

where the viscosity of the melt, η_{melt}, is Newtonian and depends on temperature and composition; η_r, the relative viscosity, depends on the volumetric abundance and aspect ratio of the particles as well as on the strain-rate of the flow. Here, the apparent viscosity of the lava is calculated using a combination of thermodynamic and empirical rheological models. A viscosity value is thereby obtained considering the interstitial melt composition and the amount of crystals given by MELTS at every degree from above the liquidus until the solidus (full crystallisation).

The viscosity of the interstitial liquid is estimated via the GRD model (Giordano et al., 2008). This model was chosen over other models (e.g., Shaw, 1969; Bottinga and Weill, 1972; Hui and Zhang, 2007) because it considers a wider range of chemical compositions and includes the non-Arrhenian temperature dependence of silicate melt viscosity following the Vogel–Fulcher–Tammann equation (Vogel, 1921; Fulcher, 1925; Tammann and Hesse, 1926):

$$\log \eta_{melt} = A + \frac{B(\chi)}{T - C(\chi)} \tag{10}$$

where A is a constant representing the lower limit of silicate melt viscosity at high temperature; and B and C are fitting parameters depending on chemical composition (Giordano et al., 2008). The fitting parameters are calculated from the melt composition given by MELTS at every temperature step.

The particle effect is calculated using three rheological models: Shaw (1969), Krieger and Dougherty (1959) and Costa et al. (2009; via Cimarelli et al., 2011), focusing only on the effects of the crystalline phases. Although vesicles are present in our samples, and bubbles have likely affected the flow behaviour (e.g., Pinkerton and Sparks, 1978; Lipman et al., 1985), at present there exists no general law describing their complete effect on the apparent viscosity of a bubbly lava (Stein and Spera, 1992; Quane and Russell, 2005; Pistone et al., 2012), and therefore they are not considered here.

The Shaw model is an attempt to quantify the effect of crystals using the Einstein–Roscoe equation:

$$\eta_r = (1 - 1.35\phi)^{-2.5} \tag{11}$$

This equation may be applied only for dilute concentrations of spherical particles (implicitly assuming a theoretical maximum packing fraction of 0.74). The second model proposed by Krieger and Dougherty (1959) is derived from the Einstein–Roscoe equation and accounts for particle shape:

$$\eta_r = 1 - \left(\frac{\phi}{\phi_m}\right)^{B\phi_m} \tag{12}$$

where ϕ_m represents the maximum random packing fraction for a given particle size and shape distribution (e.g., Mueller et al., 2010). The maximum packing fraction is the maximum crystal fraction achieved by accumulation of randomly oriented solids. B is called the Einstein coefficient. Using this model, the effect of a mixture of coarse and fine particles may be approximated by the product of the relative effect of each particle type (Farris, 1968):

$$\eta_r = \eta_r(\phi_c) \times \eta_r(\phi_f) \tag{13}$$

For both, Eq. (11) and Eq. (12), the analytical expression predicts a sharp viscosity increase when the solid fraction approaches the maximum packing, commonly associated with the onset of apparent yield strength (Zhou et al., 1995; Hoover et al., 2001; Saar et al., 2001). When considering time-scales shorter than those required to observe deformation, rheological studies have therefore employed Bingham flow laws, accounting for a yield strength (see Barnes, 1999). Under such conditions, the relationship between yield strength and particle volume fraction has been previously tested but the answer is not unique (Castruccio et al., 2010). The five most common equations are given in Appendix A1 (Table A.1) and are used here to calculate the yield strength as function of the total crystal fraction given by MELTS.

After sufficiently long time-scales, the behaviour of crystal-bearing magmas is better described by a shear-thinning law with a strain-rate dependency and absence of yield strength (e.g., Caricchi et al., 2007; Lavallée et al., 2007). The third model that is used here is the one proposed by Costa (2005) and Costa et al. (2009), which is based on a semi-empirical non-Newtonian relationship for dilute- to highly-concentrated polydisperse suspensions, taking into account the shape of the particles and the strain-rate dependency:

$$\eta_r(\phi) = \frac{1 + \left(\frac{\phi}{\phi_m}\right)^{\delta}}{\left[1 - F\left(\frac{\phi}{\phi_m}, \xi, \gamma\right)\right]^{B\phi_m}} \tag{14}$$

with F given by:

$$F = (1 - \xi)\, erf\left[\frac{\sqrt{\pi}}{2(1-\xi)}\frac{\phi}{\phi_*}\left(1 + \frac{\phi^{\gamma}}{\phi_*^{\gamma}}\right)\right] \tag{15}$$

The error function erf describes a rheological transition below and above the maximum packing limit. The model of Costa is used here with fitting parameters given in Cimarelli et al. (2011) based on analogue experiments of polydisperse suspensions consisting of coarse, equant particles and fine, prolate particles in a bubble-free Newtonian liquid (analogous to the interstitial silicate melt). This parameterisation has adjustable parameters depending on the amount of finer particles with regard to coarser particles ($x = \phi_f/(\phi_f + \phi_c)$) and on adjustable independent parameters for the two types of suspension:

$$\begin{aligned} \phi_{*cf} &= \phi_{*f} x^{1.34} + \phi_{*c}(1-x)^{1.34} \\ \gamma_{cf} &= \gamma_f x + \gamma_c (1-x) \\ \xi_{cf} &= \xi_f x + \xi_c (1-x) \end{aligned} \tag{16}$$

Both for the Krieger–Dougherty and Costa models, the relative viscosity is calculated considering a bi-modal mixture with the coarse particles being modelled as spheres to mimic the effect of olivine phenocrysts and the fine particles being modelled as needles to mimic the effect of microlites, in a bubble-free Newtonian interstitial silicate melt. Ultimately, the relative viscosity and the apparent yield strength are calculated at each temperature increment according to the crystal volume fraction correspondingly obtained via MELTS.

3. Results

3.1. Description of the flow morphology

In proximal 2 km, smooth, flat lava surfaces, ropy textures and multiple collapsed roofs reveals pahoehoe type lava emplaced as tube-fed flow. About 2 km from the vent, the lava advanced through a narrow passage between two hyaloclastite mounds (informally named 'bottleneck') and flows down a steep scarp (Fig. 1d). This slope break appears to have locally enhanced the lava velocity and caused the lava surface to stretch and brecciate into a crumbly to blocky a'a-type flow. Below the scarp, no evidence of tubes was found but irregular blocks of tens of centimetre forming a clinkery texture typical of a'a type. Downstream of the bottleneck and the change in slope the flow velocity appears to have abruptly waned, partially causing the formation of pressure ridges and inflation features. About 800 m downstream of the bottleneck the bulk of the flow stops, forming a broad flow lobe from which a breakout yields the extrusion of a narrow flow tongue. Although the whole lava flow is interpreted as volume-limited (as observed by drained lava tubes at proximal reaches), the distal portion of the flow (the last 2 km) is interpreted as a cooling limited flow due to undrained channel and distal breakout (Wilson and Head, 1994). A weakly visible, filled-channel faces with levees is only observed over a short flow length of about 20 m (profile 6, Fig 2). Consequently, the distal portion represents a cooling-limited flow system. Due to the tube-fed regime and the complex emplacement of the proximal to medial flow portions, geometric flow parameters and resulting lava flow viscosity and yield strength were determined for the distal part of the lava flow downstream of the bottleneck (Fig. 2).

3.2. Viscosity estimate from flow morphological dimensions

A total of nine cross-flow profiles were analysed where flow width, height and length were measured (Fig. 2, Table 2). Each profile is an average of ten individual measurements spaced one meter apart. The lava flow segment has a length of 2044.7 ± 0.8 m; its width varies from 124.7 m to 359.7 m with an average width of 218.6 ± 0.3 m and its height ranges from 2.1 m to 7.5 m with an average of 4.73 ± 0.28 m. Propagation of even small errors in

Table 2
Geometric flow parameters and resulting lava flow viscosity and yield strength.

Physical constant				
ρ [kg m^{-3}]		2600 ± 100		
g [m s^{-2}]		9.80665		
G_z [−]		300		
κ [m^2 s^{-1}]		7×10^{-7}		
Average of all profiles	**Mean**	**Error**	**% Error**	
W [m]	218.6	0.3	0.10	
w [m] (for profile 6)	103.2	1.5	1.50	
L [m]	2044.66	0.82	0.04	
H [m]	4.73	0.28	5.10	
α [°]	1.66	0.00	0.10	
Rheological parameter	**Mean**	**Error**	**% Error**	
Q [m^3 s^{-1}]	19.9	0.567	2.86	Eq. (2)
$\eta_{flow,1}$ [Pa s]	2.86×10^5	5.12×10^4	17.88	Eq. (3)
$\eta_{flow,2}$ [Pa s]	6.41×10^5	1.54×10^5	23.97	Eq. (4)
$\eta_{flow,3}$ [Pa s]	5.98×10^3	1.12×10^3	18.70	Eq. (8)
$\tau_{0,flow,1}$ [Pa]	3.49×10^3	2.40×10^2	6.88	Eq. (5)
$\tau_{0,flow,2}$ [Pa]	4.68×10^3	2.72×10^2	5.81	Eq. (6)
$\tau_{0,flow,3}$ [Pa]	2.10×10^3	2.65×10^2	12.60	Eq. (7)

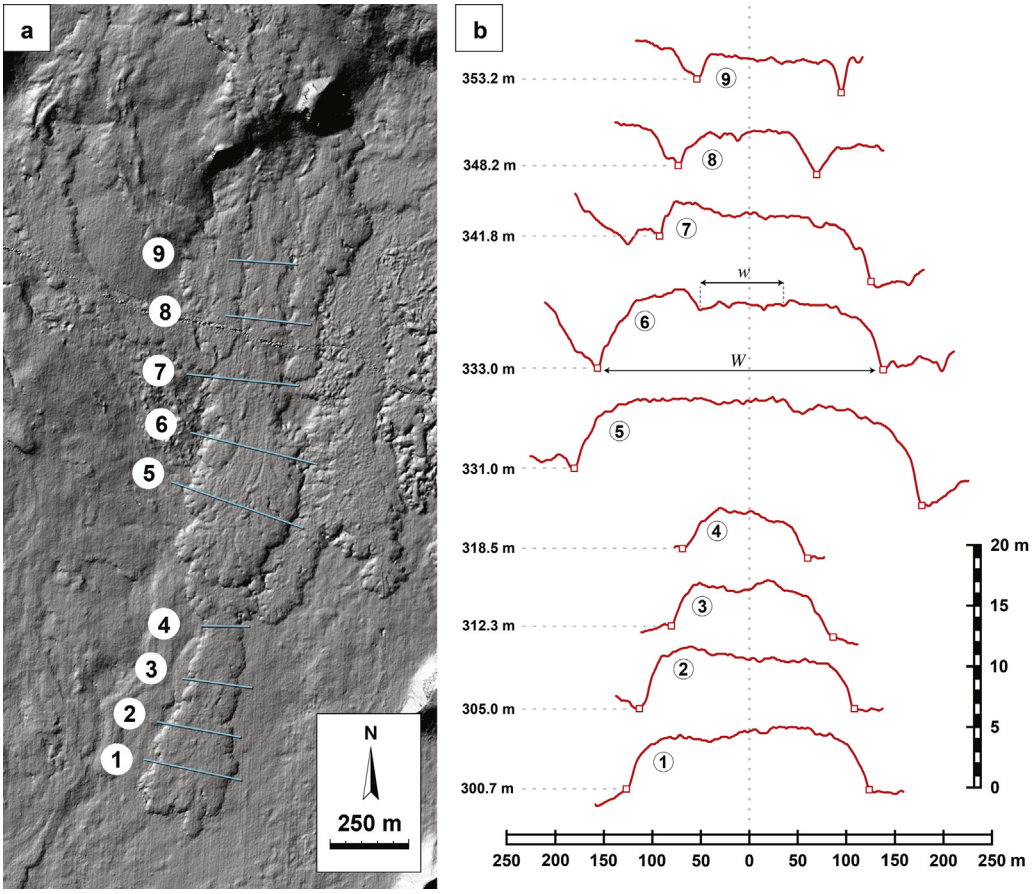

Fig. 2. (a) Data Elevation Model of the distal section of lava flow with location of the profiles used to estimate the rheological parameters. (b) Topography cross-section of the profiles with vertical exaggeration. Numbers on the left side are the absolute elevation at the bottom of the profiles.

Table 3
Normalised bulk rock geochemical compositions and petrological characteristics of the samples. Bulk rock analyses were carried out at the Service d'Analyse des Roches et des Minéraux (Nancy, France) via Inductively Coupled Plasma Optical Emission Spectrometry (ICP-OES) technique. Details of the methodology and uncertainties of this technique can be found in Carignan et al. (2001). Oxide abundances are in wt.% and FeO_{tot} is the total Fe expressed as FeO.

	L2D	L2B1	L2B2	L2G	L2A	Average	Stdev
SiO_2	48.17	48.15	47.94	48.04	48.16	48.09	0.10
TiO_2	1.75	1.74	1.74	1.73	1.75	1.74	0.01
Al_2O_3	15.00	14.78	14.85	14.82	14.89	14.87	0.08
FeO_{tot}	12.03	12.17	12.18	12.10	12.07	12.11	0.06
MnO	0.20	0.21	0.21	0.21	0.21	0.21	0.00
MgO	8.72	8.92	9.15	9.06	8.72	8.92	0.20
CaO	11.63	11.55	11.45	11.55	11.69	11.57	0.09
Na_2O	2.11	2.10	2.11	2.12	2.13	2.11	0.01
K_2O	0.20	0.20	0.21	0.20	0.20	0.20	0.00
P_2O_5	0.17	0.17	0.17	0.17	0.17	0.17	0.00
Total	100.00	100.00	100.00	100.00	100.00	100.00	
Mg #	0.62	0.63	0.63	0.63	0.62	0.63	
% Vesicles	20.07	12.67	16.18	12.90	15.99	15.56	
% Olivine	1.77	4.44	2.32	7.55	1.33	3.48	
% Plagioclase	7.92	4.62	2.89	2.99	1.58	4.00	

Mg # = Mg100 / (Mg + Fe).

morphometric parameters measurements may cause a large spread in the rheological properties. In particular, the variation in flow height significantly affects the error on viscosity and yield strength calculations, as it is factored by a power of 3 and 4 (see for example Eqs. (3) and (4)). The topographic gradient was determined adjacent to the lava flow where the underlying topography is exposed as well as on the flow surface where the pre-eruption topography is concealed by adjacent flows. The average underlying slope is about 1.66°. Error analysis includes formal statistical errors (see Appendix A.2 for details and Lefler, 2011) for both morphometric variations using repeated measurements and absolute instrumental parameters.

The calculated effusion rate is 19.9 ± 0.56 $m^3 s^{-1}$ (Eq. (2)). The flow viscosities obtained using Eq. (3) and Eq. (4) are on the order of 10^5 Pa s. In contrast, Eq. (8) provides a viscosity value two orders of magnitude lower (5.98×10^3 Pa s). The geometrical analysis thus provides a wide range of possible nominal viscosity estimates. On the other hand, the estimates of apparent yield strength of the flow varies slightly between 2.1 and 4.68×10^3 Pa (Eqs. (5), (6), (7)) and the errors remain less than 12.6% irrespective of the equation considered.

3.3. Chemistry and petrography

The bulk rock chemistry of the samples shows compositional homogeneity and petrographic analyses reveal no systematic variations in the volume fraction of vesicles and crystals along the flow (Table 3). The lava is basaltic in composition with 48 wt.% SiO_2, less than 2.5 wt.% alkali, and a Mg # of 0.63. Like most hot-spot related basaltic material, the total iron content is fairly high with 12 wt.% FeO_{tot}.

The rocks exhibit a glomeroporphyritic texture with clusters of euhedral olivine phenocrysts and some interlocking plagioclase surrounded by a microcrystalline groundmass (Fig. 3). Vesicle diameters range from 50 μm to more than a few millimetres, and the phenocrysts are up to 1 mm in length, sometimes occurring in clusters of up to 5 mm in diameter. Point counting reveals that all samples are comprised of, on average, 12 to 20 vol.% vesicles and 3 to 10 vol.% pre-eruptive phenocrysts (with lengths exceeding 200 μm). The remaining groundmass fraction, as detailed through back-scattered electron images (Fig. 3), exhibits an intergranular texture in which olivine and pyroxene and at a later stage, oxides, fill the interstices of a framework formed by tabular plagioclase microlites of less than 200 μm (representing about 50% of the groundmass). No interstitial glass could be identified (as is often the case for basaltic lava). Within a single sample, however, the vesicle volume fraction locally varied and the bubble shape could occasionally change from spherical to elongate/stretched bubbles and microlites locally show a fluidal alignment along a flow direction and around the bubbles, suggesting strain localisation and/or heterogeneity in volatile content and/or temperature (Fig. 3e). Although these local variations may result in a complex flow regime, we neglect their effects with respect to the rheological behaviour of the lava flow as a whole during flow emplacement.

3.4. Crystallisation sequence

3.4.1. Optical observation and thermometry

In our analysis, we follow the common belief that phenocrysts formed in the magma chamber, whereas the microlites crystallised during magma ascent, eruption and subsequent flow emplacement (e.g., Gill, 2010). The temperature of the onset of olivine crystallisation is calculated using the 'olivine-liquid thermometer' (Putirka, 2008) in which the core of the olivine is considered to be in equilibrium with a liquid having the bulk rock composition. Using the chemical compositions of the olivine core (given in Appendix A.3) and assuming a pressure of 1 kbar, and presence of 0.4 wt.% H_2O in the magma chamber (Eason and Sinton, 2009), the temperature of the liquidus is estimated to be 1215 °C.

Interpretation of the textural analyses suggest that olivine is the first mineral to crystallise in the magma chamber, followed by plagioclase and that eruption has occurred at, or immediately after, the onset of plagioclase crystallisation, because there are less than 1 vol.% plagioclase phenocrysts within the sample. The groundmass (liquid phase prior to eruption) crystallises quickly during magma ascent and lava flow emplacement. During magma ascent and eruption the drop of pressure within the magma drives gas exsolution and nucleation of bubbles that enhance crystallisation. Such forced crystallisation generates abundant microlites of plagioclase and iron-rich olivine, tens of micrometres in size in the groundmass. Subsequently, the residual liquid crystallised as clinopyroxene and oxides.

3.4.2. Thermodynamic calculator

The thermodynamic calculator MELTS is used to describe the abundance of each crystalline and liquid phase during magma ascent, eruption and emplacement at every temperature step (Fig. 4). The starting chemical composition considered here is obtained by averaging the bulk-rock composition of the samples. In the magma chamber, at 1 kbar, 0.4 wt.% H_2O and QFM-2 (Eason and Sinton, 2009), the appearance of olivine would occur at 1213 °C (consistent with the estimation from the thermobarometer of Putirka,

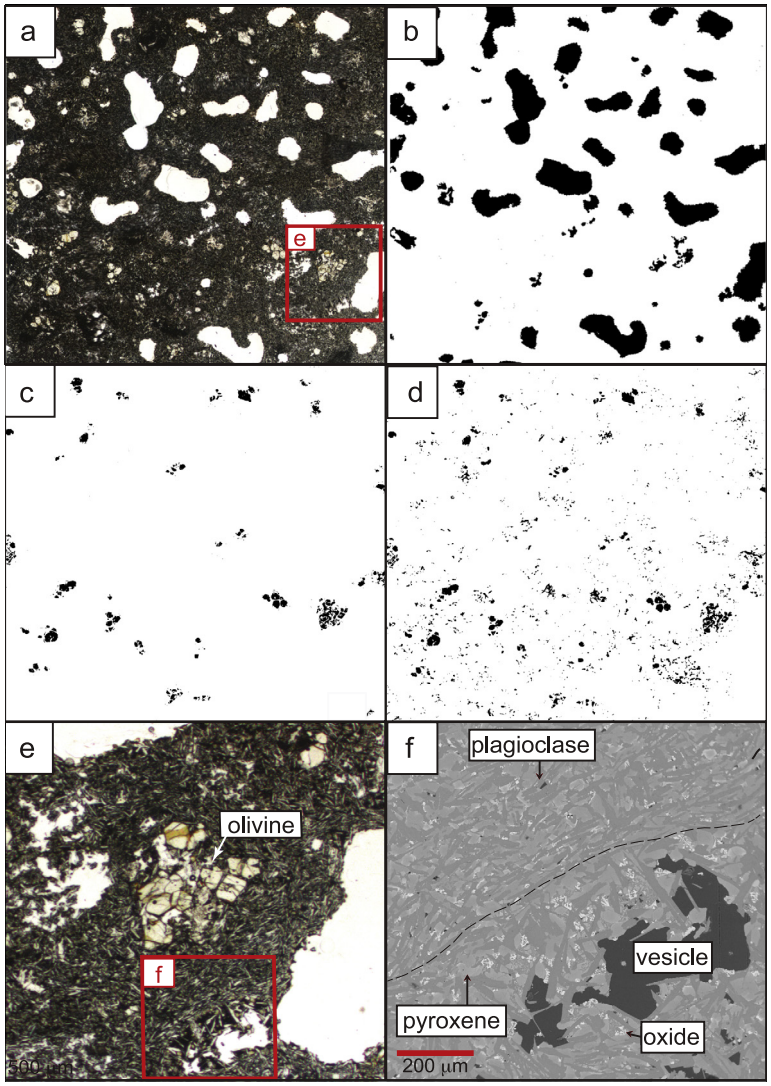

Fig. 3. Petrographic analyses of the sample L2A. (a) Photograph in plane-polarised light; and associated binary images used to evaluate the vol.% of: (b) vesicles, (c) olivine phenocrysts and (d) all crystals larger than 200 μm. (e) Closer look at the thin section shows the petrographic assemblage and (f) back scattered electron analyses (using a CAMECA SX100 Electron MicroProbe Analyser) evidences the microcrystalline groundmass with pyroxene crystallised in between the plagioclase microlites and the oxides at last in the remaining space; the plagioclase microlite laths are aligned in a flow direction. In this example, plagioclase (in dark grey) represents 50% of the total area of this picture.

Table 4
Fit parameters for sphere-like and needle-like particles independent on strain rate (Mueller et al., 2010) used in Eq. (12) and for diverse strain-rate (Cimarelli et al., 2011) used in Eqs. (14), (15) and (16). [Note: the parameters at 10^{-6} s^{-1} are extrapolated using the strain-rate dependency offered by Caricchi et al., 2007.]

	Mueller et al. (2010)		Cimarelli et al. (2011)					
			at 10^{-6} s^{-1}		at 10^{-4} s^{-1}		at 1 s^{-1}	
	Sphere	Needle	Sphere	Needle	Sphere	Needle	Sphere	Needle
ϕ_m	0.641	0.343	0.61	0.26	0.54	0.36	0.61	0.44
δ			11.539	9.653	11.48	7.5	2.79	4.541
γ			1.4609	3.347	1.52	5.5	1.6	8.55
ϕ_*			0.5317	0.25	0.62	0.26	0.67	0.28
ξ			3.8×10^{-5}	2.2×10^{-4}	5×10^{-3}	2×10^{-4}	10×10^{-3}	1×10^{-3}

2008), followed by plagioclase at 1180 °C. The eruptive temperature is suggested to be 1175±5 °C, based on the extent of crystallisation required to produce the phenocryst content observed in the rock. The ascent of the magma is modelled by decreasing pressure from 1 kbar to 1 bar while maintaining a constant temperature of 1175 °C and oxygen fugacity at QFM-2. During the pressure drop, MELTS computes a loss of water from 0.4 to 0.06 wt.% and an increase in crystallinity from 7 to 19 vol.%. The late-stage crystallisation is calculated at 1 bar and QFM-2 until the solidus temperature is reached. The onset of Ca-rich pyroxene nucleation occurs at 1170 °C, and oxides crystallise at 1108 °C from the remaining liquid. Complete crystallisation is achieved at 1095 °C (solidus temperature).

3.5. Transient viscosity model of the crystallising lava flow

The transient apparent viscosity of the erupted material is calculated using Eq. (9), based on the viscosity of the residual liquid calculated via the GRD model and the relative viscosity estimated using three different models: Shaw (1969), Krieger and Dougherty

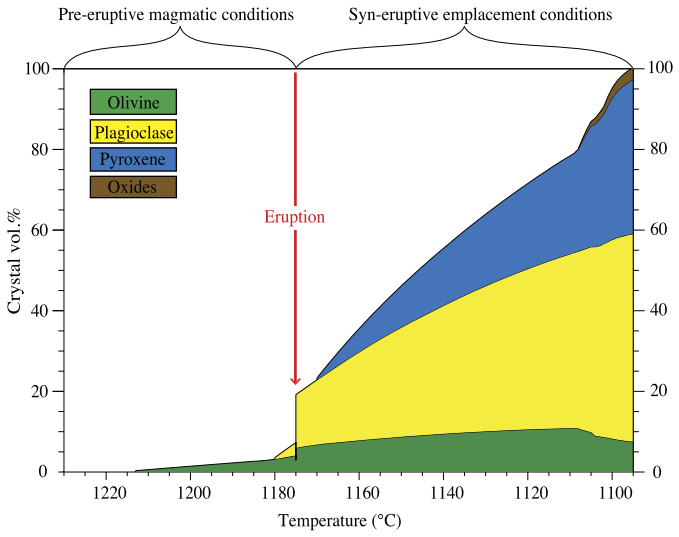

Fig. 4. Crystallisation sequence as a function of temperature calculated with MELTS from the magma chamber conditions (1 kbar, 0.4 wt.% H_2O, QFM-2) through isothermal eruption and emplacement at the surface (1 bar, QFM-2).

(1959) and Costa (via Cimarelli et al., 2011). For the Shaw method, all crystals are considered identical with spherical shape. For the Krieger–Dougherty method, the relative viscosity was calculated using fitting parameters from Mueller et al. (2010), considering the product of coarse spherical particle to model the olivine phenocrysts (with a maximum packing of 0.64) and needles-like fine particles to model microlites (with a maximum packing of 0.34) (Table 4). For the calculation using the Costa equation (Eqs. (14), (15), (16)), the relative viscosity was calculated using the fitting parameters given in Table 4 from Cimarelli et al. (2011) for strain rates of 10^{-6}, 10^{-4} and 1 s^{-1}, according to the relative proportions, x, of phenocrysts (spheres) and microlites (needles).

The calculated apparent viscosity obtained through all three models is presented as a function of temperature in Fig. 5. The viscosity of the molten bulk rock and of the residual liquid (η_{melt}) calculated at each temperature (using the GRD model) are also shown. These curves can be used to distinguish between the effect of the compositional change in the residual melt and the effect of crystals. [Note: the viscosity of the molten bulk rock was experimentally measured on a melted sample using the concentric cylinder method (Dingwell, 1986). At superliquidus conditions, the apparent viscosity is similar to the viscosity of the remelted whole rock.]

At the onset of olivine crystallisation, the apparent viscosity becomes progressively higher than the bulk liquid's viscosity. The large increase in plagioclase and the water loss due to magma ascent of the lava at the eruption result in a sharp increase in viscosity. Under post-eruption conditions, during cooling at the Earth's surface, the apparent viscosity continuously increases with microlite nucleation and growth. The Shaw and Krieger–Dougherty models compute a sharp viscosity increase when approaching the maximum packing values and fails to compute viscosity for lower temperatures at which the crystal content exceeds the maximum packing because they mathematically lead to infinite values. In contrast, the model provided by Costa enables us to quantify the remaining rheological evolution of the crystallising lava above the critical crystal fraction where the mixture behaviour is controlled by the solid network.

3.6. Yield strength of the crystallising lava flow

Pure silicate liquids have no yield strength, so the dependence of the yield strength with temperature is only due to the increas-

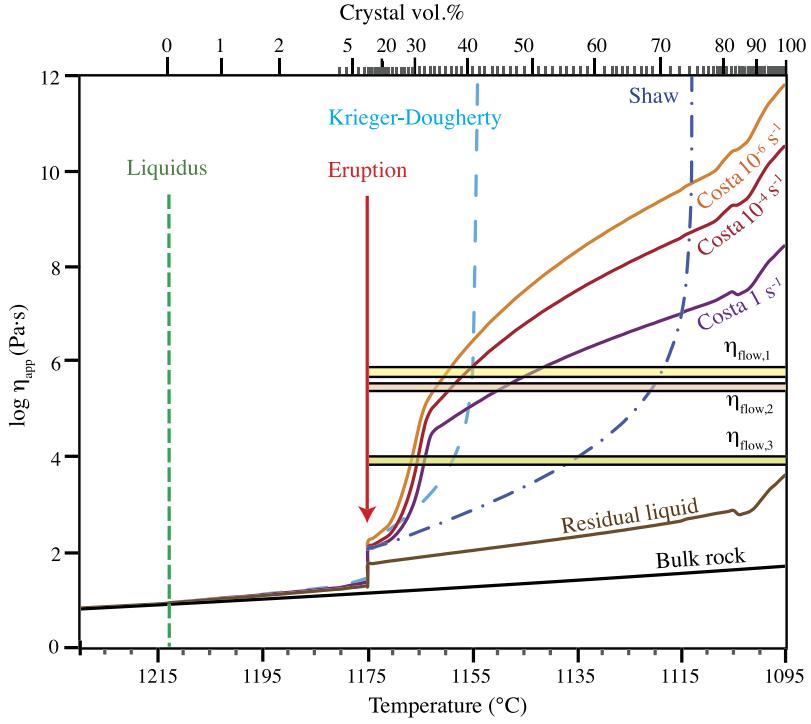

Fig. 5. Apparent viscosity of the crystallising lava as a function of temperature and corresponding crystallinity modelled with MELTS. The apparent viscosity is calculated according to three models: Shaw (1969) using Eq. (12) that considers all crystals are spheres (dashed dark blue line); Krieger and Dougherty (1959) using Eq. (13) that considers the sum of the effect of the mafic minerals modelled as spheres and of plagioclase modelled as needles (light blue dashed line); and Costa et al. (2009) using Eqs. (14), (15), (16) considering the parameterisation of Cimarelli et al., 2011 for a mixture of mafic minerals (modelled as spheres) and plagioclase (modelled as needles) for strain rates of 10^{-6}, 10^{-4} and 1 s^{-1} (orange, red and purple line respectively). The liquid's viscosity of the bulk-rock (black line) and the residual liquid viscosity (brown line) are also represented. The apparent viscosity of the flow obtained from the geometric parameters, $\eta_{flow,1}$, $\eta_{flow,2}$ and $\eta_{flow,3}$ calculated using Eq. (3) and Eq. (4) and Eq. (8) respectively, are represented independently of the crystallisation sequence (coloured areas correspond to the associated uncertainties of the values).

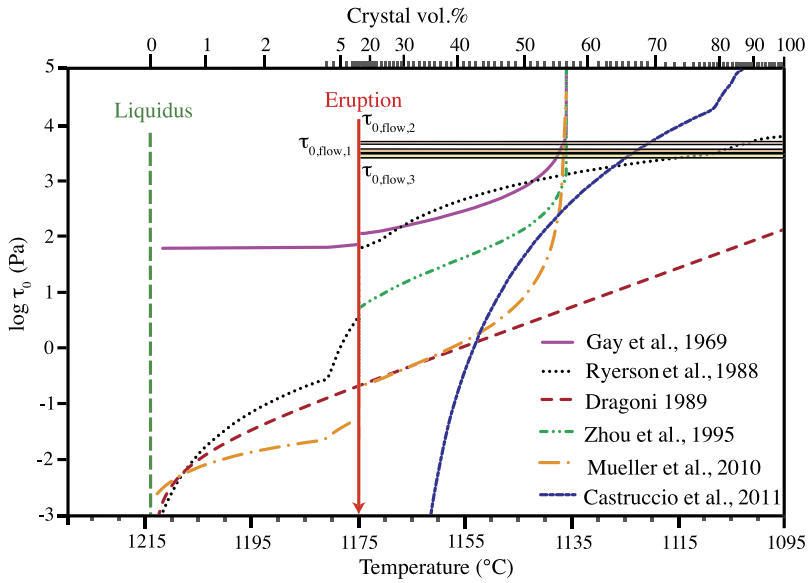

Fig. 6. Apparent yield strength of the crystallising lava as a function of the temperature and corresponding crystallinity modelled by MELTS. The lava's yield strength is calculated as a function of crystal content using the various models available in the literature (see Appendix A1). As an attempt to account for the effect of bi-modal particles, the calculated yield strength was calculated as the product of the yield strength due to the mafic crystals (modelled as spheres-like shape) and plagioclase (modelled as needle-like shape): $\tau_0 = \tau_{0(\text{mafic})}\ \tau_{0(\text{plagioclase})}$ with $\phi_m = 0.64$ and $\phi_c = 0.3$ for mafic minerals and $\phi_m = 0.34$ and $\phi_c = 0.09$ for plagioclase. The apparent yield strength obtained from the geometric parameters of the lava flow, $\tau_{0,flow,1}$, $\tau_{0,flow,2}$ and $\tau_{0,flow,3}$ using Eqs. (5), (6) and (7), respectively are represented independently of the crystallisation sequence (coloured areas correspond to the associated uncertainties of the values).

ing crystal content (Fig. 6). Depending on the model, the mixture may start to exhibit yield strength as soon as crystals form (Gay et al., 1969; Ryerson et al., 1988; Dragoni, 1989; Mueller et al., 2010), whereas other models consider a minimum crystal content before onset of the yield strength (Zhou et al., 1995; Castruccio et al., 2010). A sharp increase of the yield strength is first observed due to the onset of plagioclase crystallisation and then due to further crystallisation after eruption, and eventually, in some cases it is extrapolated to infinite when crystallinity reaches the maximum packing (Gay et al., 1969; Zhou et al., 1995; Mueller et al., 2010). In contrast, the experimental fit of Ryerson et al. (1988) and Castruccio et al. (2010), which does not consider a maximum packing value, reaches a maximum value of the order of $10^{3.5}$ to 10^5 Pa.

4. Discussion

Here we use rheological models and thermodynamic calculation to describe the full path of lava rheology during cooling upon eruption until its full crystallisation. The solution is, however, not unique in that a given mineral assemblage (with specific ratios of minerals) can be achieved through crystallisation of a range of parental magmas using diverse initial conditions. Moreover, MELTS is intransigent to disequilibrium crystallisation kinetics typical of volcanic environments. Owing to our ability to sample the studied lava flow, our model revolves around well-constrained geochemical conditions; yet, it certainly does not fully account for crystallisation disequilibrium associated with rapid cooling. Crystallisation is considered in equilibrium, but the crystal shape for microlites was considered to be elongate, which typifies rapid cooling conditions. Future improvement will require the coupling of cooling rate and crystal growth (rate, shape and size) with rheology to measure the change of viscosity as a function of the distance from the source vent and as a function of vertical location within the flow. In that sense, various cooling rates and differences in the degree of crystallisation between base, surface and core of the flow must be accounted for. Thus, the assumption of thermodynamic equilibrium between all the crystal phases and the liquid, and at each temperature step, is a simplification employed here in a volcanic environment.

4.1. Comparison of morphological and petrological methods

Other studies have previously attempted to estimate the apparent viscosity as function of the crystallisation sequence (e.g., Shaw, 1969; Ryerson et al., 1988; Pinkerton and Stevenson, 1992; Harris and Allen, 2008). These studies employed earlier empirical models describing the viscosity of liquids (e.g., Shaw, 1972; Bottinga and Weill, 1970) as well as the Einstein–Roscoe equation to determine the effect of crystals. Although these combined methods provide reasonable approximations at low crystal contents (<20 vol.%) associated with near-liquidus temperatures (e.g., Ishibashi and Sato, 2007; Vona et al., 2011), they fail to map the complete rheological evolution of crystallising lava until solidification (crossing of the solidus temperature). The comparative model analysis introduced in the present study illustrates how each of the three main models (Shaw, 1969; Krieger and Dougherty, 1959; and Costa et al., 2009), given a set of parameters (pressure, temperature, chemistry, crystal content and shape, etc.) can provide contrasting apparent viscosity estimates (see Fig. 5). When trying to constrain the rheological evolution of lava undergoing complete crystallisation, the model of Costa (using the fitting parameters for a bi-disperse mixture from Cimarelli et al., 2011) provides, to date, the most complete viscosity description, taking into consideration any crystal fraction, varied crystal shapes, and most importantly, strain rate. The shallowing of the viscosity–crystallinity relationship above the critical crystal fraction (as described by Costa's model) suggests that in heavily loaded suspensions, deformation is strongly controlled by the crystalline network. Strain may induce crystal alignment and more particles can be accommodated as we may observe in the lava sample (Fig. 3f). The percentage area covered by the of aligned plagioclase amounts to approximately 50% that is higher than the random maximum packing for needle-like particles, a fact which emphasises the need to consider flow at degrees of crystallisation beyond the maximum packing.

The estimated single-value of viscosity and the estimated yield strength from the flow morphological dimensions overlap with the

values estimated from the crystallisation sequence when approaching the maximum packing, or just above the values corresponding to the critical crystal fraction in the case when using the model of Costa. This crystal content corresponds to the rheology of the flow where it is becoming governed by the solid particles, marked by the change of slope in the Costa model. This is the rheological limit at which the lava is too viscous to continue to flow (for this given strain-rate). This suggests that the flow has recorded in its morphology the highest viscosity and yield strength when it is becoming seemingly stagnant. We wish to emphasise that in the case of polycrystalline magmatic suspensions, the crystals with the highest aspect ratio control this critical crystal fraction: higher crystal aspect ratios lead to lower critical crystal fraction. The rheological values estimated from the morphology are therefore highly sensitive to the crystal fraction and importantly the crystal shape (hence the crystalline phases).

In the context of a cooling and crystallising basaltic flow, the yield strength increases until it reaches the value corresponding to the time-scale for which the flow appears to be stagnant. In other words, the yield strength of a lava flow is an "apparent value" that is defined by the lava flow's final morphological dimensions. Previous attempts to model the relationships between shear strength and crystallinity reflect the time-scale of the experimental procedures. In many investigations, the slower strain rate approaches 10^{-6} s^{-1}, which, in some models, agree on a yield strength around 10^3 to 10^4 Pa (e.g., Gay et al., 1969; Ryerson et al., 1988; Zhou et al., 1995; Mueller et al., 2010)—a range similar to the values obtained from flow morphology characteristics (Fig. 6).

Our results imply that the geometrical approximation of single viscosity and yield strength values (as described by Jeffreys' and Hulme's equations) cannot accurately constrain the details of a flow's rheological evolution. Although it may help to distinguish between extremes (e.g., mafic vs. felsic flows), the non-unique rheological/petrological path evolution may prevent our ability to distinguish more subtlety between lava flow compositions. The difficulties may be even more significant when considering apparent high-viscosity flows. Protracted extrusion of andesitic lava domes at Volcán de Colima, Mexico, for example, have been constrained to flow at viscosities of 10^{10}–10^{12} Pa s (Lavallée et al., 2012)—a viscosity range which, according to Walker (1973) and Pinkerton and Wilson's (1994) scheme, would suggest a rhyolitic origin. In the latter, the sequence of crystallisation may not be the decisive factor influencing the rheological evolution of the flow, but rather its general cooling and degassing (e.g., Hess et al., 2005). As lava degasses, its viscosity increases which in turn slows down the rate of structural relaxation of the lava, forced to undergo the glass transition. Such lava will thus be subject to a different rheological evolution, that may not depend so strongly on crystallisation sequence.

4.2. Implications for the rheological mapping of extra-terrestrial lava flows

In the present study, the basaltic, iron-rich, Icelandic lava flow is taken as an analogue for basaltic martian lava flows. One may therefore assume a somewhat similar crystallisation sequence and, thus, similar viscosity evolution during emplacement on Mars although cooling rate, oxygen fugacity, atmospheric pressure and degassing efficiency may temperate direct comparison. The range of lava viscosities calculated on Mars may therefore reflect differences in bulk composition together with different cooling history and crystallisation sequence. The high viscosity values (10^5–10^6 Pa s) calculated for martian lava flows may be best explained by basaltic compositions, as suggested by remote sensing compositional data, with high crystal content (>50 vol.%) and not necessarily by more silicic composition. Such lava may be expected to behave like an a'a type flow, similar to the distal portion of the studied Icelandic flow. In the case of some martian lava flows with low inferred viscosity values ($<10^3$ Pa s), high effusion rates (>100 m^3 s^{-1}) or low silica content may favour the extreme long run-out distances of such lava, as previously proposed by Vaucher et al. (2009). Such low viscosities may also be explained by rapid crystallisation of high aspect ratio, needle-like crystals, as observed in Komatiitic spinifex textures that would favour very low maximum packing value. This would in turn effectively slow the lava at high temperature and thus yield a freezing-in at low apparent viscosity. Spinifex textures have been suggested for martian lavas, based on crystallisation experiments of basaltic rocks analysed in-situ by Mars Exploration Rovers (Bost et al., 2012). Lava flows with seemingly low viscosities, associated with recent ultramafic volcanism in Central Elysium Planitia (e.g., Stockstill-Cahill et al., 2008), may preserve such textures. The value for optical description of petrographic textures of igneous rocks imaged by rovers during landing missions is apparent here. In this context, the interpretation of martian flows should combine morphological analysis with the mineralogical observation from high-resolution visible and near-infrared spectroscopy. Using such multidisciplinary approach may significantly reduce uncertainties on lava flow compositions and rheological behaviour during flow emplacement.

5. Conclusion

The viscosity of a lava flow of the Western Volcanic Zone in Iceland has been estimated from its morphology via the methodology typically used in planetary sciences. In order to evaluate the physical meaning of such estimates, we have constrained the transient rheology of the erupted lava considering the observed crystallisation sequence, further modelled through MELTS based on chemical composition, crystal content and shape, and geothermobarometric data. The viscosity is shown to depend strongly on the crystallisation sequence. The results demonstrate that the flow viscosity is inevitably transient and increases by more than 6 orders of magnitude during emplacement from the vent to the flow front. The lava viscosity quickly becomes non-Newtonian as the groundmass crystallises. Using combined thermodynamic and empirical models, which consider both, the composition and morphology of crystals, is an important step towards improved viscosity estimates. We show that rheological properties obtained from the morphology of the flow are distinct from the lava behaviour at the eruption onset and during most of its emplacement, corresponding rather to transient values occurring near flow cessation.

The present comparative approach should be applied to a wide range of compositions (andesitic, dacitic) in order to verify the use of such a method in planetary sciences. Complementary analyses (e.g., radar, direct sampling) should be employed to constrain potential geochemical differences. We recommend that thermodynamic calculations and rheological models be deployed in tandem to better understand the complex behaviour of extra-terrestrial lava flows. In the case of Mars, where volcanic rocks' chemical and mineralogical compositions are becoming relatively well constrained through the ages (e.g., Baratoux et al., 2011; Grott et al., 2013), such a combined morphological/rheological/petrological approach may prove invaluable to study the surface expression of the planet's geodynamics.

Acknowledgements

M.O. Chevrel wishes to thank THESIS (Elitenetzwerk Bayern) for financial support. T. Platz and E. Hauber were partially supported by the Helmholtz association through the research alliance "Planetary evolution and life". The authors wish to thank Elena Lefler for

her work on error propagation during the calculation of rheological parameters presented as B.Sc. thesis (Freie Universität Berlin). D.B. Dingwell acknowledges the research professorship of the Bundesexzellenzinitiative (LMUexcellent) and an Advanced Grant of the European Research Council (EVOKES–247076). D. Baratoux acknowledges funding from the Programme National of Planétologie (INSU). Y. Lavallée acknowledges funding from the Deutsche Forschungsgemeinschaft (LA2651/1-1 and LA2651/3-1) as well as the Starter Grant of the European Research Council (SLiM–306488).

Appendix A. Supplementary material

Supplementary material related to this article can be found online at http://dx.doi.org/10.1016/j.epsl.2013.09.022.

References

Bagdassarov, N., Dingwell, D.B., 1992. A rheological investigation of vesicular rhyolite. J. Volcanol. Geotherm. Res. 50, 307–322.
Bagdassarov, N.S., Dingwell, D.B., Webb, S.L., 1994. Viscoelasticity of crystal-bearing and bubble-bearing rhyolite melts. Phys. Earth Planet. Inter. 83, 83–99.
Baloga, S.M., Mouginis-Mark, P.J., Glaze, L.S., 2003. Rheology of a long lava flow at Pavonis Mons, Mars. J. Geophys. Res. 108, 5066.
Baratoux, D., Toplis, M.J., Monnereau, M., Gasnault, O., 2011. Thermal history of Mars inferred from orbital geochemistry of volcanic provinces. Nature 472, 338–341.
Barnes, H.A., 1999. The yield stress—a review or 'panta roi'—everything flows? J. Non-Newton. Fluid Mech. 81, 133–178.
Basaltic Volcanism Study Project, 1981. Basaltic Volcanism on the Terrestrial Planets. Pergamon Press, Inc., New York, 1286 pp.
Bost, N., Westall, F., Gaillard, F., Ramboz, C., Foucher, F., 2012. Synthesis of a spinifex-textured basalt as an analog to Gusev crater basalts, Mars. Meteorit. Planet. Sci., 1–12.
Bottinga, Y., Weill, D.F., 1972. The viscosity of magmatic silicate liquids: A model for calculation. Am. J. Sci. 272, 438–475.
Caricchi, L., Burlini, L., Ulmer, P., Gerya, T., Vassalli, M., Papale, P., 2007. Non-Newtonian rheology of crystal-bearing magmas and implications for magma ascent dynamics. Earth Planet. Sci. Lett. 264, 402–419.
Carignan, J., Hild, P., Mevelle, G., Morel, J., Yeghicheyan, D., 2001. Routine analyses of trace element in geological samples using flow injection and low pressure on-line liquid chromatography coupled to ICP-MS: a study of geochemical reference materials BR, DR-N, UB-N, AN-G and GH. Geostand. Newsl. 25, 187–198.
Cashman, K.V., Thornber, C., Kauahikaua, J.P., 1999. Cooling and crystallisation of lava in open channels, and the transition of Pahoehoe Lava to 'A'a. Bull. Volcanol. 61, 306–323.
Castruccio, A., Rust, A.C., Sparks, R.S.J., 2010. Rheology and flow of crystal-bearing lavas: Insights from analogue gravity currents. Earth Planet. Sci. Lett. 297, 471–480.
Cimarelli, C., Costa, A., Mueller, S., Mader, H.M., 2011. Rheology of magmas with bimodal crystal size and shape distributions: Insights from analog experiments. Geochem. Geophys. Geosyst. 12, Q07024.
Costa, A., 2005. Viscosity of high crystal content melts: Dependence on solid fraction. Geophys. Res. Lett. 32, L22308.
Costa, A., Caricchi, L., Bagdassarov, N., 2009. A model for the rheology of particle-bearing suspensions and partially molten rocks. Geochem. Geophys. Geosyst. 10.
Crisp, J., Cashman, K.v., Bonini, J.A., Hougen, S., Pieri, D., 1994. Crystallization history of the 1984 Mauna Loa lava flow. J. Geophys. Res. 99, 7177–7198.
Dingwell, D.B., 1986. Viscosity-temperature relationships in the system $Na_2Si_2O_5$–$Na_4Al_2O_5$. Geochim. Cosmochim. Acta 50, 1261–1265.
Dingwell, D.B., 2006. Transport properties of magmas diffusion and rheology. Elements 2, 281–286.
Dragoni, M., 1989. A dynamical model of lava flows cooling by radiation. Bull. Volcanol. 51, 88–95.
Eason, D.E., Sinton, J.M., 2009. Lava shields and fissure eruptions of the Western Volcanic Zone, Iceland: Evidence for magma chambers and crustal interaction. J. Volcanol. Geotherm. Res. 186, 331–348.
Farris, R.J., 1968. Prediction of the viscosity of multimodal suspensions from unimodal viscosity data. Trans. Soc. Rheol. 12, 281–301.
Fink, J.H., Griffiths, R.W., 1992. A laboratory analog study of the morphology of lava flows extruded from point and line sources. J. Volcanol. Geotherm. Res. 54, 19–32.
Fulcher, G.S., 1925. Analysis of recent measurements of the viscosity of glasses. J. Am. Ceram. Soc. 8, 339–355.
Gay, E.C., Nelson, P.A., Armstrong, W.P., 1969. Flow properties of suspensions with high solid concentrations. AIChE J. 15, 815–822.
Ghiorso, M.S., Sack, O., 1995. Chemical mass transfer in magmatic processes IV. A revised and internally consistent thermodynamic model for the interpolation and extrapolation of liquid–solid equilibria in magmatic systems at elevated temperatures and pressures. Contrib. Mineral. Petrol. 119, 197–212.
Gill, R., 2010. Igneous Rocks an Processes: A Practical Guide. Blackwell Publishing.
Giordano, D., Polacci, M., Longo, A., Papale, P., Dingwell, D.B., Boschi, E., Kasereka, M., 2007. Thermo-rheological magma control on the impact of highly fluid lava flows at Mt. Nyiragongo. Geophys. Res. Lett. 34, L06301.
Giordano, D., Russell, J.K., Dingwell, D.B., 2008. Viscosity of magmatic liquids: A model. Earth Planet. Sci. Lett. 271, 123–134.
Glaze, L.S., Baloga, S.M., 2006. Rheologic inferences from the levees of lava flows on Mars. J. Geophys. Res. 111, E09006.
Glaze, L.S., Baloga, S.M., Stofan, E.R., 2003. A methodology for constraining lava flow rheologies with MOLA. Icarus 165, 26–33.
Gregg, T.K.P., Fink, J.H., 1996. Quantification of extraterrestrial lava flow effusion rates through laboratory simulations. J. Geophys. Res. 101, 16891–16900.
Gregg, T.K.P., Fink, J.H., 2000. A laboratory investigation into the effects of slope on lava flow morphology. J. Volcanol. Geotherm. Res. 96, 145–159.
Grott, M., Baratoux, D., Hauber, E., Sautter, V., Mustard, J., Gasnault, O., Ruff, S.W., Karato, S.-I., Debaille, V., Knapmeyer, M., Sohl, F., Van Hoolst, T., Breuer, D., Morschhauser, A., Toplis, M.J., 2013. Long-term evolution of the martian crust–mantle system. Space Sci. Rev. 174, 49–111.
Guest, J.E., Kilburn, C.R.J., Pinkerton, H., Duncan, A.M., 1987. The evolution of lava flow-fields: observations of the 1981 and 1983 eruptions of Mount Etna, Sicily. Bull. Volcanol. 49, 527–540.
Gwinner, K., Scholten, F., Preusker, F., Elgner, S., Roatsch, T., Spiegel, M., Schmidt, R., Oberst, J., Jaumann, R., Heipke, C., 2010. Topography of Mars from global mapping by HRSC high-resolution digital terrain models and orthoimages: characteristics and performance. Earth Planet. Sci. Lett. 294, 506–519.
Harris, A.J.L., Allen, J.S., 2008. One-, two- and three-phase viscosity treatments for basaltic lava flows. J. Geophys. Res. 113.
Hauber, E., Brož, P., Jagert, F., Jodlowskł, P., Platz, T., 2011. Very recent and wide spread basaltic volcanism on Mars. Geophys. Res. Lett. 38, L10201.
Hess, K.-U., Dingwell, D.B., 1996. Viscosities of hydrous leucogranitic melts: A non-Arrhenian model. Am. Mineral. 81, 1297–1300.
Hess, K.-U., Lavallée, Y., Castro, J., Noll, K., Mueller, S., Dingwell, D.B., Cameron, B.I., Spieler, O., Fink, J.H., 2005. Rheology of obsidian flow: emplacement controlled by final water degassing?. Eos Trans. AGU 85, Fall Meeting Suppl., Abstract V53C-1584.
Hiesinger, H., Head, J.W., Neukum, G., 2007. Young lava flows on the eastern flank of Ascraeus Mons: Rheological properties derived from High Resolution Stereo Camera (HRSC) images and Mars Orbiter Laser Altimeter (MOLA) data. J. Geophys. Res. 112.
Hoover, S.R., Cashman, K.V., Manga, M., 2001. The yield strength of subliquidus basalts—experimental results. J. Volcanol. Geotherm. Res. 107, 1–18.
Hui, H., Zhang, Y., 2007. Toward a general viscosity equation for natural anhydrous and hydrous silicate melts. Geochim. Cosmochim. Acta 71, 403–416.
Hulme, G., 1974. The interpretation of lava flow morphology. Geophys. J. R. Astron. Soc. 39, 361–383.
Ishibashi, H., 2009. Non-Newtonian behavior of plagioclase-bearing basaltic magma: subliquidus viscosity measurement of the 1707 basalt of Fuji volcano, Japan. J. Volcanol. Geotherm. Res. 181, 78–88.
Ishibashi, H., Sato, H., 2007. Viscosity measurements of subliquidus magmas: Alkali olivine basalt from the Higashi-Matsuura district, Southwest Japan. J. Volcanol. Geotherm. Res. 160, 223–238.
Jaeger, W.L., Keszthelyi, L.P., Skinner Jr, J.A., Milazzo, M.P., McEwen, A.S., Titus, T.N., Rosiek, M.R., Galuszka, D.M., Howington-Kraus, E., Kirk, R.L., 2010. Emplacement of the youngest flood lava on Mars: A short, turbulent story. Icarus 205, 230–243.
Jeffreys, H., 1925. The flow of water in an inclined channel of rectangular section. Philos. Mag. Ser. 6 49 (293), 793–807.
Knudson, J.G., Katz, D.L., 1958. Fluid Dynamics, Heat Transfer. McGraw-Hill, pp. 81–82.
Krieger, I.M., Dougherty, T.J., 1959. A mechanism for non-Newtonian flow in suspensions of rigid spheres. J. Rheol. 3, 137.
Lavallée, Y., Hess, K.-U., Cordonnier, B., Dingwell, D.B., 2007. Non-Newtonian rheological law for highly crystalline dome lavas. Geology 35, 843–846.
Lavallée, Y., Varley, N.R., Alatorre-Ibargüengoitia, M.A., Hess, K.-U., Kueppers, U., Mueller, S., Richard, D., Scheu, B., Spieler, O., Dingwell, D.B., 2012. Magmatic architecture of dome-building eruptions at Volcán de Colima, Mexico. Bull. Volcanol. 74, 249–260.
Lefler, E., 2011. Genauigkeitsbetrachtung bei der Ermittlung rheologischer Parameter von Lavaströmen aus Fernerkundungsdaten. B.Sc. thesis. Freie Universität Berlin, Berlin, 75 pp.
Lejeune, A.M., Bottinga, Y., Trull, T.W., Richet, P., 1999. Rheology of bubble-bearing magmas. Earth Planet. Sci. Lett. 166, 71–84.
Lejeune, A.-M., Richet, P., 1995. Rheology of crystal-bearing silicate melts: an experimental study at high viscosities. J. Geophys. Res. 100, 4215–4230.
Lipman, P.W., Banks, N.G., Rhodes, J.M., 1985. Degassing-induced crystallization of basaltic magma and effects on lava rheology. Nature 317, 604–607.
Lyman, A.W., Koenig, E., Fink, J.H., 2004. Predicting yield strengths and effusion rates of lava domes from morphology and underlying topography. J. Volcanol. Geotherm. Res. 129, 125–138.
Manga, M., Castro, J., Cashman, K.V., Loewenberg, M., 1998. Rheology of bubble-bearing magmas. J. Volcanol. Geotherm. Res. 87, 15–28.

Moore, H.J., Arthur, D.W.G., Schaber, G.G., 1978. Yield strengths of flows on the Earth, Mars, and Moon. In: Proc. Lunar Planet. Sci. Conf. 9th, pp. 3351–3378.
Moore, H.J., Schaber, G.G., 1975. An estimate of the yield strength of the Imbrium flows. In: Proc. Lunar Sci. Conf. 6th, pp. 101–118.
Mueller, S., Llewellin, E.W., Mader, H.M., 2010. The rheology of suspensions of solid particles. Philos. Trans. R. Soc. Lond. A 466, 1201–1228.
Nichols, R.L., 1939. Viscosity of lava. J. Geol. 47, 290–302.
Pasckert, J.H., Hiesinger, H., Reiss, D., 2012. Rheologies and ages of lava flows on Elysium Mons, Mars. Icarus 219, 443–457.
Petford, N., 2009. Which effective viscosity?. Mineral. Mag. 73, 167–191.
Pinkerton, H., 1987. Factor affecting the morphology of lava flows. Endeavour 11, 73–79.
Pinkerton, H., Norton, G., 1995. Rheological properties of basaltic lavas at sub-liquidus temperatures: laboratory and field measurements on lavas from Mount Etna. J. Volcanol. Geotherm. Res. 68, 307–323.
Pinkerton, H., Sparks, R.S.J., 1976. The 1975 sub-terminal lavas, Mount Etna: a case history of the formation of a compound lava field. J. Volcanol. Geotherm. Res. 1, 167–182.
Pinkerton, H., Sparks, R.S.J., 1978. Field measurements of the rheology of lava. Nature 276, 383–385.
Pinkerton, H., Stevenson, R.J., 1992. Methods of determining the rheological properties of magmas at sub-liquidus temperatures. J. Volcanol. Geotherm. Res. 53, 47–66.
Pinkerton, H., Wilson, L., 1994. Factor controlling the lengths of channel-fed lava flows. Bull. Volcanol. 6, 108–120.
Pistone, M., Caricchi, L., Ulmer, P., Burlini, L., Ardia, P., Reusser, E., Marone, F., Arbaret, L., 2012. Deformation experiments of bubble- and crystal-bearing magmas: Rheological and microstructural analysis. J. Geophys. Res. 117, B05208.
Putirka, K., 2008. Thermometers and barometers for volcanic systems. In: Putirka, K., Tepley, F. (Eds.), Minerals, Inclusions and Volcanic Processes. In: Rev. Mineral. Geochem., vol. 69. Mineralogical Soc. Am, pp. 61–120.
Quane, S., Russell, J.K., 2005. Welding: Insights from high-temperature analogue experiments. J. Volcanol. Geotherm. Res. 142, 67–87.
Ryerson, F.J., Weed, H.C., Piwinskii, A.J., 1988. Rheology of subliquidus magmas: I. Picritic compositions. J. Geophys. Res. 93, 3421–3436.
Saar, M.O., Manga, M., 1999. Permeability–porosity relationship in vesicular basalts. Geophys. Res. Lett. 26, 111–114.
Saar, M.O., Manga, M., Cashman, K.V., Fremouw, S., 2001. Numerical models of the onset of yield strength in crystal-melt suspensions. Earth Planet. Sci. Lett. 187, 367–379.
Sato, H., 2005. Viscosity measurement of subliquidus magmas: 1707 basalt of Fuji volcano. J. Mineral. Petrol. Sci. 100, 133–142.
Scholten, F., Gwinner, K., Roatsch, T., Matz, K.-D., Wählisch, M., Giese, B., Oberst, J., Jaumann, R., Neukum, G., 2005. Mars Express HRSC data processing—methods and operational aspects. Photogramm. Eng. Remote Sens. 71, 1143–1152.
Shaw, H.R., 1969. Rheology of basalt in the melting range. J. Petrol. 10, 510–535.
Shaw, H.R., 1972. Viscosities of magmatic silicate liquids: An empirical method of prediction. Am. J. Sci. 272, 870–893.
Sinton, J., Grönvold, K., Sæmundsson, K., 2005. Postglacial eruptive history of the Western Volcanic Zone, Iceland. Geochem. Geophys. Geosyst. 6, Q12009.
Stein, D.J., Spera, F.J., 1992. Rheology and microstructure of magmatic emulsions: Theory and experiments. J. Volcanol. Geotherm. Res. 49, 157–174.
Stein, D.J., Spera, F.J., 2002. Shear viscosity of rhyolite-vapor emulsions at magmatic temperatures by concentric cylinder rheometry. J. Volcanol. Geotherm. Res. 113, 243–258.
Stockstill-Cahill, K.R., Anderson, F.S., Hamilton, V.E., 2008. A study of low-albedo deposits within Amazonis Planitia craters: Evidence for locally derived ultramafic to mafic materials. J. Geophys. Res. 113.
Tammann, G., Hesse, W., 1926. Die Abhängigkeit der Viskosität von der Temperatur bei unterkühlten Flüssigkeiten. Z. Anorg. Allg. Chem. 156, 245–257.
Vaucher, J., Baratoux, D., Toplis, M.J., Pinet, P., Mangold, N., Kurita, K., 2009. The morphologies of volcanic landforms at Central Elysium Planitia: Evidence for recent and fluid lavas on Mars. Icarus 200, 39–51.
Vogel, D.H., 1921. Temperaturabhängigkeitsgesetz der Viskosität von Flüssigkeiten. Phys. Z. 22, 645–646.
Vona, A., Romano, C., Dingwell, D.B., Giordano, D., 2011. The rheology of crystal-bearing basaltic magmas from Stromboli and Etna. Geochim. Cosmochim. Acta, 3214–3236.
Walker, G.P.L., 1973. Lengths of lava flows. Philos. Trans. R. Soc. Lond. 274, 107–118.
Warner, N.H., Gregg, T.K.P., 2003. Evolved lavas on Mars? Observations from southwest Arsia Mons and Sabancaya volcano, Peru. J. Geophys. Res. 108.
Wilson, L., Head, J.W., 1994. Mars review and analysis of volcanic eruption theory and relationships to observed landforms. Rev. Geophys. 32, 221–263.
Wilson, L., Mouginis-Mark, P.J., Tyson, S., Mackown, J., Garbeil, H., 2009. Fissure eruptions in Tharsis, Mars implications for eruption conditions and magma sources. J. Volcanol. Geotherm. Res. 185, 28–46.
Zhou, J.Z.Q., Fang, T., Luo, G., Uhlerr, P.H.T., 1995. Yield stress and maximum packing fraction of concentrated suspensions. Rheol. Acta 34, 544–561.
Zimbelman, J.R., 1985. Estimates od rheologic properties for flows on the Martian Volcano Ascraeus Mons. J. Geophys. Res. 90, D157, D162.
Zimbelman, J.R., 1998. Emplacement of long lava flows on planetary surfaces. J. Geophys. Res. 103, 27,503–527,516.

Further reading

Platz, T., Cronin, S.J., Smith, I.E.M., Turner, M.B., Stewart, R.B., 2007. Improving the reliability of microprobe-based analyses of andesitic glasses for tephra correlation. Holocene 17, 573–583.
Pouchou, J.L., Pichoir, F., 1985. 'PAP' procedure for improved quantitative microanalysis. In: Microbeam analysis. San Francisco Press, San Francisco, pp. 104–160.